

Electrochemical oxidation of titanium by pulsed discharge in electrolyte

S.K. Poznyak^a, D.V. Talapin^b, A.I. Kulak^{c,*}

^a *Research Institute for Physical Chemical Problems, Belarusian State University, Leningradskaya St. 14, 220050 Minsk, Belarus*

^b *Institute of Physical Chemistry, University of Hamburg, Grindelallee 117, 20146 Hamburg, Germany*

^c *Institute of General and Inorganic Chemistry, National Academy of Sciences of Belarus, Surganova St. 9, 220072 Minsk, Belarus*

Received 5 November 2004; received in revised form 1 March 2005; accepted 6 March 2005

Available online 12 April 2005

Abstract

We propose a high-voltage (>1000 V) pulsed discharge method of preparation of thin anodic films on valve metals under conditions of extremely high rates of the film growth. The peculiarities of this method have been demonstrated on the anodic oxidation of titanium in sulfuric acid solutions.

A light flash at the electrode was generated upon the pulsed anodization of titanium. The emission spectra consist of narrow lines assigned to electronically excited O, H and Ti atoms, indicating that a hot plasma is created at the electrode surface. The current efficiency of TiO₂ anodic film formation exceeds markedly 100% for the pulsed Ti anodization. This non-faradaic yield was associated with the contribution of the plasma-generated high-energy radicals to the oxide growth processes. We applied various techniques to compare the composition, morphology, structure and semiconducting properties of the anodic films prepared by the high-voltage pulsed discharge and the conventional galvanostatic anodization. The anodic TiO₂ films prepared by the high-voltage pulsed discharge have nearly ideal stoichiometric composition and are more amorphous as compared to galvanostatically grown ones. Thin TiO₂ films (50–150 nm) formed in the pulsed regime exhibit significantly higher photocurrent quantum yields at $\lambda < 310$ nm and a significantly lower donor concentration.

© 2005 Elsevier B.V. All rights reserved.

Keywords: Titanium dioxide; Photoelectrochemistry; Anodic oxide films; Semiconductor oxide; Semiconductor-electrolyte interfaces; High-voltage discharge anodizing

1. Introduction

The anodic oxidation of valve metals, such as Al, Ta, Nb, Zr, Ti, etc., is studied for many years since the anodic oxide films are of great interest mainly due to their application for capacitor manufacturing and for metal protection against corrosion [1]. Comprehensive studies of the kinetics of anodic oxide film growth, as well as their physical and chemical properties have been reviewed in a number of reports [2–7]. The characteristics

of anodic films were shown to be strongly dependent on the film formation conditions (electrical regime of oxidation, oxidation time, composition and temperature of electrolyte, etc.).

The anodic films are typically prepared using dc polarization of a valve metal electrode under potentiostatic, galvanostatic or potentiodynamic control. In most of the cases, a compact barrier-type film is initially formed on the valve metal. As the thickness of oxide film reaches a certain (critical) value, the film is broken through due to impact or tunneling ionization [8–11]. Although the breakdown of anodic layers is considered to be harmful because, as a rule, it results in the degradation of their dielectric and protection characteristics,

* Corresponding author. Tel.: +375 17 2841723; fax: +375 17 2842703.

E-mail address: kulak@igic.bas-net.by (A.I. Kulak).

this phenomenon gave rise to development of a new technology of metal treatment termed “micro-plasma oxidation” or “plasma electrolytic oxidation (PEO)” [12–14]. This technique operates at potentials above the breakdown voltage of an anodic film and is characterized by luminescence sparks moving over the treated surface. Owing to plasma thermochemical interactions in the multiple surface discharges, this method allows obtaining a wide range of the film composition and properties and, therefore, is considered as technologically promising [14]. Anodic layers prepared by the PEO technique are usually rather thick (from fractions of a micron to tens or hundreds of microns) because a barrier-type film is needed to be formed on a metal before the spark discharge processes can be observed on the electrode surface.

The present paper describes a pulsed discharge method for producing thin anodic films with a thickness ranging from nanometers to a micron. In this method, the metal oxidation proceeds under the action of single high-voltage (>1000 V) pulses on an electrode system. Under these conditions, hot plasma can be formed not only in local spots, but over the whole electrode surface. We demonstrated this method using titanium as a substrate because titanium and related alloys are the corrosion resistant materials of current practical interest [4]. Furthermore, the formed anodic passivating layer, TiO_2 , is a semiconducting material, what allowed us to study its electronic properties by electro- and photoelectrochemical methods [7,15]. In this work, we compare the morphology, structure, composition and electronic properties of the anodic oxide films on titanium, which were prepared by the conventional galvanostatic method (hereafter referred to as GS films) and the pulsed discharge one (hereafter referred to as PD films).

2. Experimental

The working electrodes were made from 1.5 mm titanium plates (99.8% Ti). The surface of the samples was mechanically and then chemically (in a hot $\text{HF}:\text{HNO}_3$ mixture, 2:3 in volume) polished to a high mirror finish, and finally rinsed thoroughly with doubly distilled water. The unexposed part of the electrodes was isolated with epoxy resin, leaving an area of about 6 cm^2 open to solution.

A schematic diagram of the experimental setup used for the pulsed discharge oxidation of metals in solution and for registration of transient characteristics of the process is shown in Fig. 1. The plasma oxidation of the metal electrode was performed by the capacitor discharge into an electrode system consisting of a working electrode, a counter electrode and an electrolyte. The capacitor bank charged to a definite voltage and the electrode system were commutated by a magnetic relay

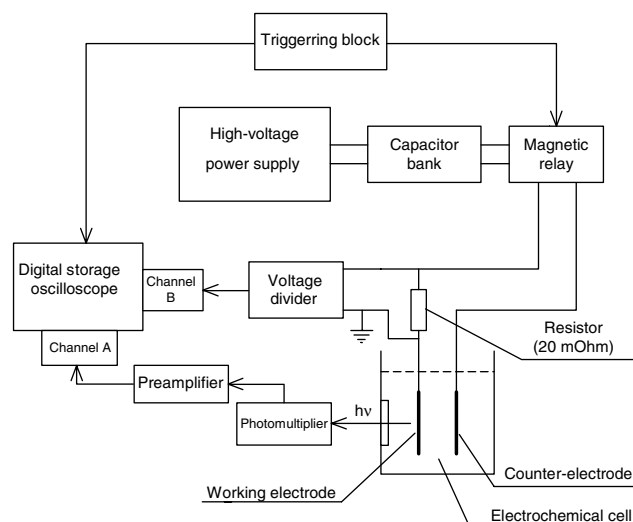


Fig. 1. A scheme of the experimental setup for the pulsed discharge electrooxidation of metals allowing recording current and emission transients.

triggered by a synchronizing pulse. Most of experiments were carried out using a capacitor of $100 \mu\text{F}$. To measure the transient current in the electrode system, a precision resistor ($20 \text{ m}\Omega$) was connected in series to the circuit and the potential drop on the resistor was recorded. To reduce ohmic losses in the system, the electrochemical cell was connected to the capacitor by low-impedance cables of minimum length. The light emitted from the working electrode under the discharge conditions was detected by a photomultiplier tube connected a fast preamplifier. A focusing system with neutral filters for the emitted light attenuation was placed between the cell and photomultiplier tube. Emission spectra were recorded using a photodiode array spectrometer SL 40-2-3648 USB covering the wavelength range from 200 to 1100 nm with a resolution of 0.5 nm.

An electrochemical cell was constructed from optically transparent high-impact polystyrene. Cylindrical titanium electrode of 2 cm in diameter with a slit was used as a counter-electrode. The surface area of this electrode was 20 times larger than that of the working electrode. The working electrode was placed in the center of the counter one so that the emitted light reached the photomultiplier tube through the slit. $1 \text{ M H}_2\text{SO}_4$ aqueous solution prepared using doubly distilled water and analytical-grade reagent was used as an electrolyte in the cell.

The conventional galvanostatic oxidation of the titanium electrode was carried out in the same cell at a current density of 10 mA cm^{-2} up to the desire voltage using a constant current power supply.

The depth-composition profile of the anodic films was obtained by the Auger spectroscopy method using a Perkin–Elmer PH-660 spectrometer. The phase composition of the films was determined by the Raman spectroscopy and X-ray diffraction methods. The Raman spectra of TiO_2 films were measured using a

Spex Ramalog 4 spectrometer and excitation by argon laser radiation of 514.5 nm. X-ray diffraction analysis of the films was performed on a HZG-4M diffractometer (Carl Zeiss) using Co K α -radiation (Mn filter). The surface morphology was studied by the scanning electron microscopy (SEM) using a Philips SEM 515 microscope. Specular reflectance spectra of the films were measured using Cary 500 UV–Vis–NIR spectrometer (Varian).

Photoelectrochemical measurements were carried out in a standard two-compartment three-electrode cell equipped with an optical quality quartz window. A platinum counter electrode and an Ag|AgCl|KCl (saturated) electrode as the reference electrode (+0.201 V vs. SHE) were used in this cell. All potentials were determined with respect to this reference electrode and controlled by a conventional potentiostat. The counter-electrode compartment was separated from the working electrode one by a fine glass frit. The photocurrent measurements were made at room temperature in 1 M H₂SO₄ solution.

Photocurrent spectra were obtained using a setup equipped with a high-intensity grating monochromator, 1000 W xenon lamp and a slowly rotating light chopper (0.3 Hz). The system was calibrated by an optical power meter and spectral dependences of the photocurrent were corrected for the spectral intensity distribution at the monochromator output.

The differential capacitance of the anodic TiO₂ films was measured at a frequency of 1 kHz using an impedance bridge (with a series equivalent circuit) connected to the potentiostat. In this case, a four-electrode cell with an additional Pt electrode with a very large surface area was used. A small a.c. signal (<10 mV rms) was superimposed to the electrode potential. Impedance measurements were performed in 1 M H₂SO₄ solution deaerated with purified argon. The thickness of the anodic films on titanium was estimated using Auger profiling data.

3. Results and discussion

3.1. Current and emission transients during the pulsed discharge

A rapid discharge process occurs in the electrode system upon switching a charged capacitor to the electrochemical cell. When a positive voltage is applied to the working electrode, the current discharge results in the growth of oxide film on the electrode surface. The capacitor is disconnected from a charging circuit at the instant of commutation, and only the energy, $W = CU_c^2/2$, stored in the capacitor charged to a voltage U_c , is dissipated during the discharge process.

Typical current transients in the circuit after commutation are shown in Fig. 2. Initially the current increases with time, reaches its peak value within 9–10 μ s and then drops. The peak position, its value and the peak half-

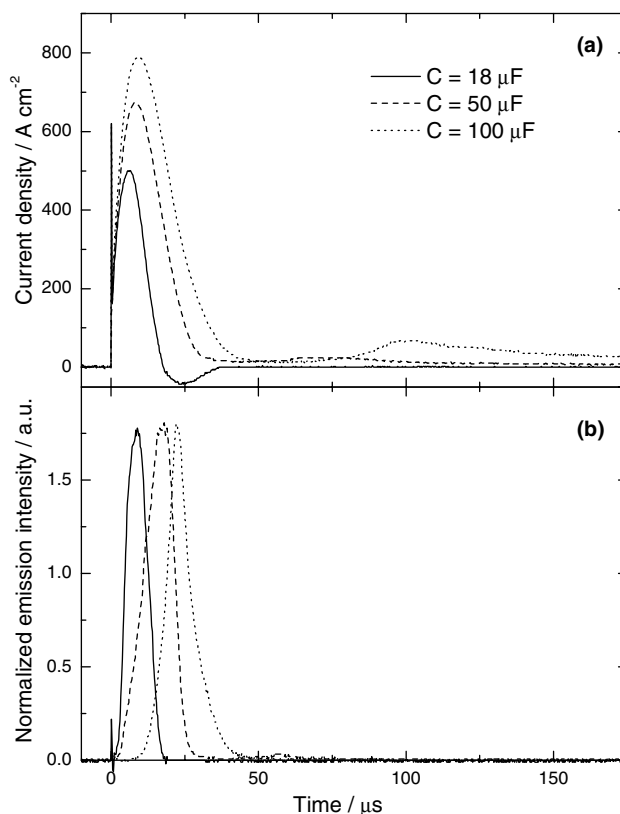


Fig. 2. Time evolution of the current (a) and emission intensity (b) when a pulse of 1350 V is applied to the Ti anode in 1 M H₂SO₄ solution. Values of a capacitor commutated to the electrochemical cell are given in the legend.

width depend on both the impedance of the electrode system, the capacitance and the applied voltage. It should be noted that aside from the main peak, a second markedly lower peak is observed (within 100–130 μ s) at the current transients. For small capacitance values (less than 25 μ F), a current peak of the opposite sign is recorded after the main peak (Fig. 2). Such unusual transient behavior of the investigated system is probably associated with a complex equivalent circuit including non-linear elements of the electrochemical cell. Characteristically, the shape of the current transient changes somewhat as the anodic film grows. This change is more distinct during the first several discharges (Fig. 3(a)), indicating that the presence of the anodic film on titanium can influence markedly the relaxation process in the system.

The pulsed anodic oxidation of titanium is accompanied by a bright flash of light at the electrode surface and the generation of a shock wave. The intensity of the emitted light is low during the first several discharges and rises significantly as their number and, hence, the anodic film thickness increases (Fig. 3(b)).

Beginning with the 10th discharge ($C = 100 \mu$ F, $U_c = 1350$ V) corresponding to the anodic film thickness 150–160 nm, a rise of the light intensity slows down and after the 15–20th discharge (the film thickness above \sim 180 nm) the emission transients differ little from each

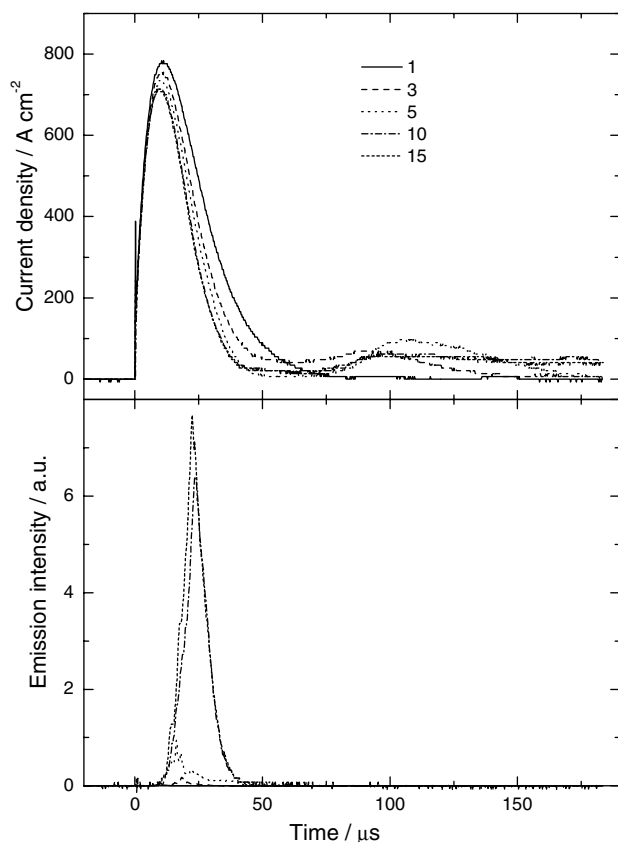


Fig. 3. Time evolution of the current (a) and emission (b) when successive pulses ($U_c = 1350$ V, $C = 100$ μ F) are applied to the Ti anode in 1 M H_2SO_4 solution. The pulse number is given in the legend.

other. Therefore, we studied the effect of the applied voltage U_c and the capacitance C on the transient processes for the electrodes pre-treated with 20 discharges. Fig. 4 shows the current and emission transients for different applied voltages (at a constant C of 100 μ F) which were recorded after pre-treatment of the titanium electrode with 20 high-voltage pulses. As the applied voltage increases, the current peak rises linearly (Fig. 4(a)), whereas the emission intensity increases very steeply (Fig. 4(b)). Integration of the light intensity over whole pulse gives the total photon flux, θ , generated by the electrode during the pulse. We observed three characteristic regions on the θ vs. U_c curve: from 50 to 500 V the value of θ rises exponentially with the U_c , then the θ depends only slightly on the U_c and above 950 V the θ again rises exponentially with increasing the applied voltage U_c .

The emission intensity increases significantly with increasing the C . The time lag in the emission peak is negligible at small C and rises up markedly with increasing the capacitance (Fig. 2(b)).

3.2. Emission spectra

Fig. 5 shows a typical emission spectrum observed for the Ti anode solution during the high-voltage discharge

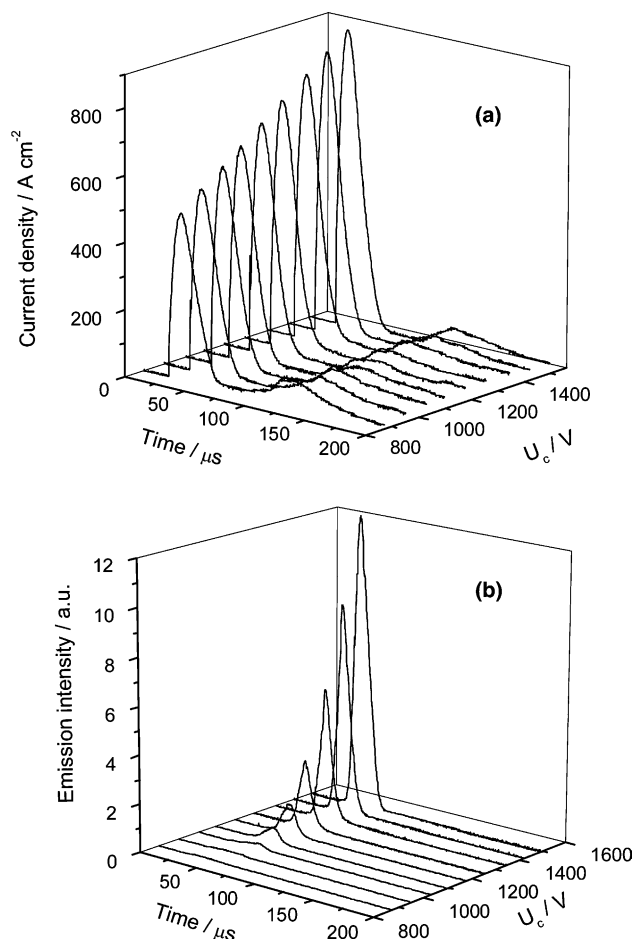


Fig. 4. (a) Current and (b) emission intensity transients recorded during the pulsed anodic oxidation of titanium electrode in 1 M H_2SO_4 solution at different applied voltages. $C = 100$ μ F. The curves were recorded after the electrode had been pre-treated with 20 discharges.

in 1 M H_2SO_4 . The spectrum comprises a number of narrow lines on a rather weak continuum background. Since the optical material (polystyrene) used for the

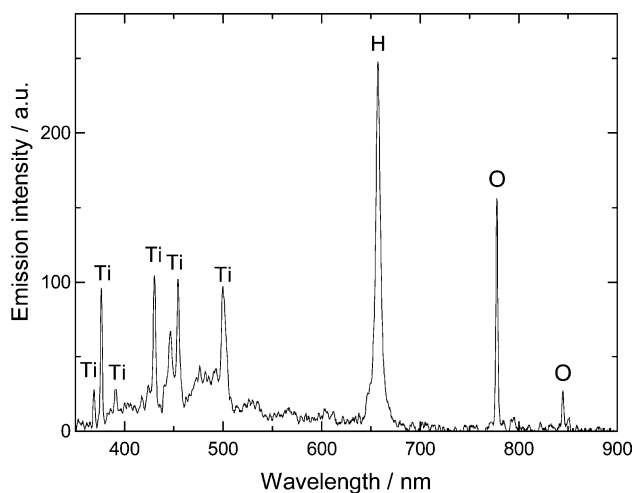


Fig. 5. Emission spectrum of a Ti anode when a pulse of 1350 V ($C = 100$ μ F) is applied to the electrochemical cell.

electrochemical cell is not transparent at wavelengths shorter than 300 nm, the emission spectrum at $\lambda < 300$ nm could not be recorded. The use of quartz optical window was found to be difficult because of shock waves generated during the discharge. All the lines present in the spectrum originate from electronically excited atoms and were earlier observed in the gas phase [16]. Thus, the emission line at 656 nm can be assigned to the Balmer series of hydrogen. The lines at 777.5 and 844 nm match well with those reported for atomic oxygen. Several emission lines observed in the region from 350 to 510 nm can be assigned to Ti atoms. Although a high concentration of SO_4^{2-} ions is present in solution, we observed no lines arising from S atoms in the emission spectrum. The linear emission spectra indicate that hot plasma involving electronically excited H and O atoms from the broken water molecules and Ti atoms from the substrate is generated near the electrode surface during the pulsed discharge.

Taking into account the experimental results obtained and the literature data on discharge phenomena in electrolytes and in pure water [14,17–19], we can suppose the following processes taking place during the high-voltage pulsed oxidation of titanium. In the case of pulsed discharges, electrochemical and plasmochemical processes at the titanium surface proceed at a relatively high input energy being approx. 100 J when switching a capacitor of 100 μF charged to 1000 V. This energy is liberated within a short period of time (20–40 μs) mostly at the titanium anode having the greatest impedance in the electrode system. As a result of the capacitor discharge, a high current density reaching 800–1000 A cm^{-2} in maximum, is observed in the circuit. In the initial step of the process, this current can result in a fast local heating of electrolyte in the near-electrode region and in its evaporation. The formation of a thin vapour film at the electrode surface during the pulsed discharge has been previously demonstrated using a high-speed camera [20]. Impact and thermal ionization of atoms and molecules will take place in the forming gas envelope, resulting in the formation of a hot plasma during the pulsed discharge. Temperature and pressure of the plasma can reach very high values. So, the plasma electron temperature as high as 13,000–15,000 K has been reported [19] for the input energies similar to those applied in the present work. In our case, the emission spectra with narrow lines, which can be assigned to electronically excited atoms of H, O and Ti in gas phase, provide strong evidence that the hot plasma is formed at the titanium electrode surface during the pulsed discharge.

3.3. Specular reflectance and Auger spectroscopy studies

During the first high-voltage discharge, a thin anodic film uniform in thickness, as reflected by uniform light

yellow interference color, is formed on the surface of a Ti electrode. The subsequent discharges result in increase of the anodic film thickness as demonstrated by a specific change of the interference color.

Studies of the reflect ion spectra of the anodic films (Fig. 6) allowed us to assume that thickness of the anodic film is different for the samples prepared by the pulsed and galvanostatic methods with the same charge passed through the electrode. To gain direct insight to the possible differences in anodic film thickness, we applied the Auger spectroscopy to determine the thickness and elemental composition of the anodic films and to estimate the film formation efficiency.

Applying the pulsed method, a total charge of 0.11 C cm^{-2} was passed through a Ti working electrode. The same charge was passed through the other Ti electrode using the galvanostatic oxidation method (a formation voltage of 30 V was reached in this experiment). Auger depth profiles of both anodic films are shown in Fig. 7(a) and (b). The oxide sputtering rate was estimated using the calibration data as $100 \pm 5 \text{ nm min}^{-1}$. The oxide film thickness was determined as the sputtering time, at which the relative atomic ratio of oxygen to titanium $N_{\text{O}}/N_{\text{Ti}}$ was 50% of the steady-state value [21], and was $68 \pm 3 \text{ nm}$ for the galvanostatically prepared film and $128 \pm 3 \text{ nm}$ for the film obtained by the pulsed method.

The thickness of anodic films is related to the charge, Q , passed during the electrochemical oxidation:

$$d = \frac{MQ\eta_f}{zF\rho S\sigma_s}, \quad (1)$$

where M and ρ are the molar mass and the density of oxide, F the Faraday constant, η_f the efficiency of film

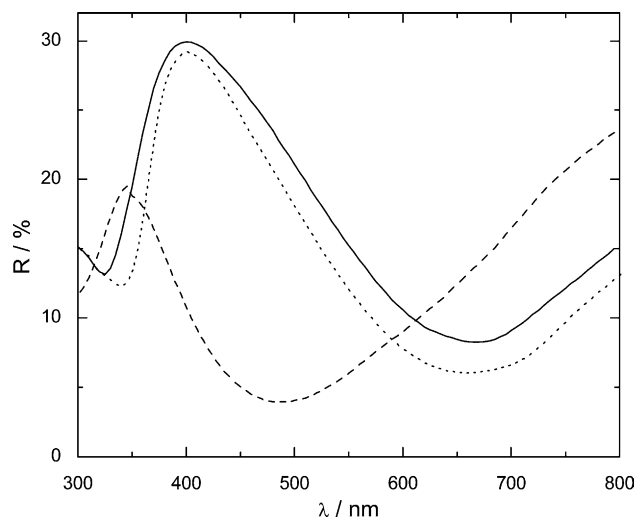


Fig. 6. Specular reflectance spectra of anodic films prepared by the pulsed anodic oxidation ($U_c = 1350 \text{ V}$, $C = 100 \mu\text{F}$, 3 discharges) (—) and the galvanostatic oxidation when the charge passed during the galvanostatic oxidation was equal to the charge passed upon the pulsed anodization (---); the galvanostatic oxidation was stopped when the color of the GS film coincided with the color of the anodic film prepared by the pulsed method (···).

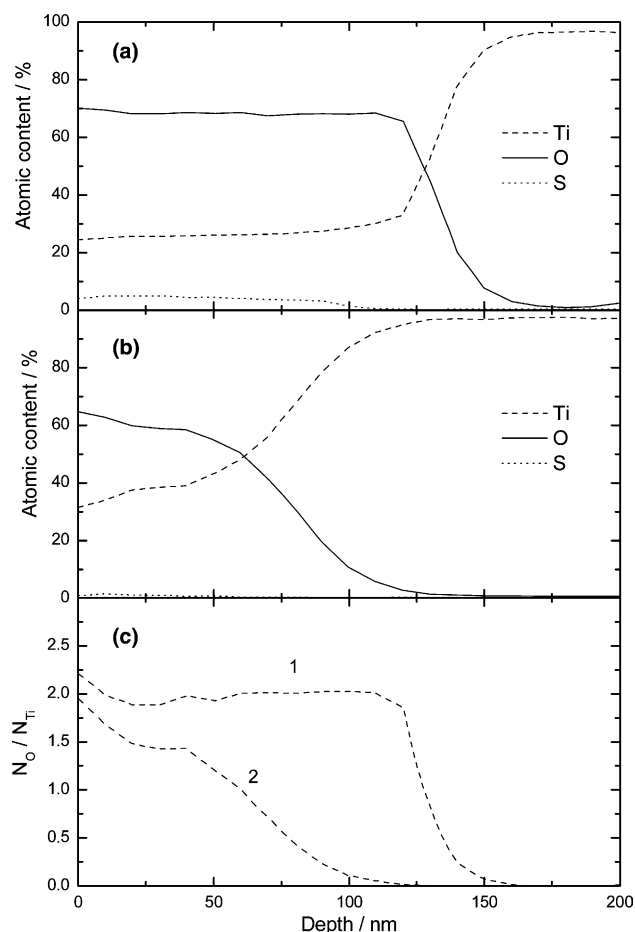


Fig. 7. Auger depth profiles of Ti, O and S atom distribution in the anodic films prepared by: (a) the pulsed discharge anodization ($U_c = 1350$ V, $C = 100$ μ F, 5 discharges); (b) galvanostatic oxidation ($j = 10$ mA cm^{-2} , $U_f = 30$ V). The charge passed through the electrode for both films was 0.11 C cm^{-2} ; (c) the depth profiles of the ratio of oxygen to titanium atomic concentrations, $N_{\text{O}}/N_{\text{Ti}}$, for the PD (1) and GS films (2). To obtain correct $N_{\text{O}}/N_{\text{Ti}}$ depth profiles, the oxygen bound with sulphur in SO_4^{2-} ions was subtracted from the total oxygen content (see text for details).

formation, S the surface area, σ_s the roughness factor of the surface and $z = 4$ for TiO_2 . Actually, z is about 3.4 for relatively thin galvanostatically grown films due to their rather high non-stoichiometry ($\text{TiO}_{1.7}$) according to Auger depth profiles of these films. Literature values of the ρ for the anodic oxide films on titanium vary in the range from 3.2 to 3.9 g cm^{-3} [10,22–25]. Taking $\rho = 3.2$ – 3.9 g cm^{-3} , $\sigma_s = 1$ for a mirror-like finishing of the electrode surface, $z = 3.4$ and $\eta_f = 1$, we can obtain $d = 68$ – 83 nm at the passed charge $Q = 0.11$ C cm^{-2} .

The thickness of the GS film estimated from the Auger profiles is slightly less than that calculated by the Eq. (1), indicating that the efficiency of the film formation can be gently less than one under galvanostatic anodization. The film formation efficiency close to one has been previously reported for the growth of titanium anodic films in sulphuric acid solutions [26]. At the same time,

the experimental value of the d for the anodic films obtained by the pulsed method is almost two times greater than the theoretically calculated value corresponding to $\eta_f = 1$ and $z = 4$. This fact is indicative of the possibility of non-faradaic behavior of titanium electrodes under conditions of the high-voltage pulsed anodization.

Non-faradaic reaction yields have been observed during the contact glow discharge electrolysis at an electrode, where a plasma is sustained by a dc glow discharge between the metal electrode and the surrounding liquid or even evaporated “gaseous” electrolyte [27–29]. This effect was attributed to the participation of high-energy radicals such as H^\cdot or OH^\cdot in reactions. These radicals can be formed from water molecules under the action of electrons and ions accelerated by the field in the near-electrode plasma. Since the pulsed anodic oxidation of titanium is performed at high voltages, it is reasonable to assume that under these conditions a plasma layer generating high-energy radicals exists at the electrode–electrolyte interface. This assumption is supported by the line emission spectrum (Fig. 5) of the electrode surface upon discharge. Chemical reactions initiated by the high-energy intermediates can be responsible for the non-faradaic efficiency of the anodic film growth during the pulsed discharge.

The analysis of Auger spectra also provides the information about the depth-dependent elemental composition of the anodic films. As shown in Fig. 7, both the GS films and the PD ones contain atoms of titanium, oxygen and sulfur, but their relative atomic ratio and the depth profiles differ for both types of anodic films. The $N_{\text{O}}/N_{\text{Ti}}$ ratio for the GS films is ~ 2 in the subsurface region. When moving from the film surface to the substrate, a region of relatively constant composition with $N_{\text{O}}/N_{\text{Ti}} = 1.5$ – 1.7 is observed and then the $N_{\text{O}}/N_{\text{Ti}}$ ratio decreases gradually, exhibiting a broad transition from oxide to metal. The content of sulfur atoms in the GS films is at the level of 1–1.5 at.%. Incorporation of sulfur into the anodic film during the galvanostatic anodization of titanium is in agreement with the literature [30–32].

The different picture is observed for the PD anodic films. The $N_{\text{O}}/N_{\text{Ti}}$ ratio varies only little throughout the film depth and is 2.5–2.7. This value is markedly higher than that expected for the TiO_2 composition. The discrepancy observed can be explained when the presence of sulfur (4–5 at.%) in the oxide film is taken into consideration. If we assume that sulfur atoms are incorporated into the anodic film as sulfate ions, this amount of sulfur can bind approx. 20 at.% of oxygen. In this case, subtraction of oxygen bound with sulfur from the total oxygen content results in the $N_{\text{O}}/N_{\text{Ti}} \approx 2$ (Fig. 7(c)), which corresponds to the stoichiometric composition of titanium dioxide. It should be noted that a transition region from TiO_2 to Ti for the PD films is markedly shorter than that for the GS films.

3.4. Morphology and structure studies

Fig. 8(a) shows an SEM micrograph of the surface of the PD anodic film obtained at a small number of discharges (≤ 5). Boundaries of titanium grains, which are also observed at freshly prepared Ti electrodes, are distinctly seen. The anodic film is homogeneous, compact and reproduces exactly a relief of the Ti substrate surface.

As the number of discharges increases (10 and more), the parts of the flowed surface well discernible at low magnifications appear (Fig. 8(b)). These patterns can arise from a strong heating and local melting of the electrode material at the instant of discharge. As can be seen on high magnification SEM image, surface the thicker films is covered with rather uniformly distributed crater-shaped hollows with an average diameter of about 100 nm (Fig. 8(c)). Similar craters were previously observed at the surface of titanium anodic films after reaching the breakdown voltage and were defined as channels of the micro-plasma discharge [12].

Thin GS films are also uniform and dense and reproduce exactly the titanium substrate morphology (Fig. 8(d)). However, according to SEM studies, the roughness of the GS films enhances with increasing the anodization time and, correspondingly, their thickness, which can be related to a gradual crystallization of the film (Fig. 8(e) and (f)).

It has been previously shown that the structure of anodic films on titanium depends considerably on the conditions of their growth, although this relationship

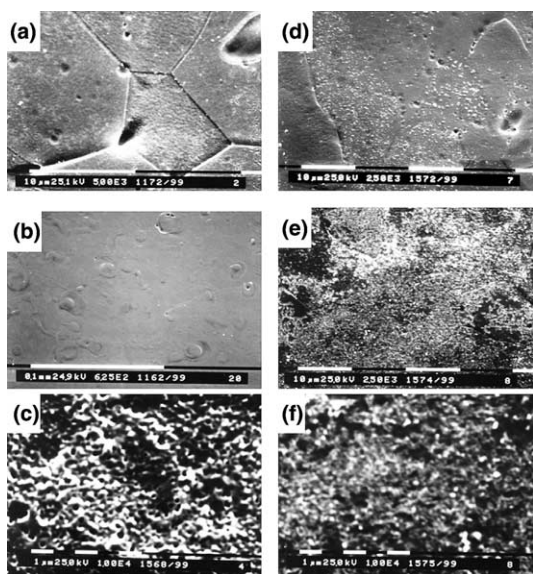


Fig. 8. (a–c) SEM micrographs of the anodic films grown on titanium by the pulsed discharge method ($U_c = 1350$ V, $C = 100$ μ F, (a) 3 discharges and (b,c) 20 discharges). (d–f) SEM micrographs of the anodic films grown galvanostatically on titanium up to $V_{\max} = 30$ V (d) and 81 V (e,f). The estimated thicknesses of the compared PD and GS films are similar (about 70 and 190 nm, respectively).

is still not clearly understood [26,32–38]. In the present work, the structure of the anodic films on titanium obtained by the pulsed discharge and galvanostatic anodization was studied by the X-ray diffraction and Raman spectroscopy methods. Thin films ($d \leq 50$ nm) prepared by both methods were revealed to be amorphous (Fig. 9(a)). Raman spectra of the thicker anodic films ($d \approx 100$ nm) display four bands at 144, 395, 512 and 645 cm^{-1} which can be assigned to the anatase structure [39,40]. Characteristically, the intensity of these bands for the GS film is higher than that for the PD film at a comparable film thickness, indicating that the latter is better crystallized (Fig. 9(a)).

Fig. 9(b) presents an XRD spectrum of a thick PD film ($d \approx 300$ nm). Besides the peaks of the titanium substrate, the peaks of anatase and rutile are observed, with a comparable content of these crystal modifications in the film.

Under the action of pulsed discharge, heat balance at the electrode surface is determined by the relationship between the rate of heat supply, Q , liberated in the near-electrode region and the rate of heat removal through the heat exchange with substrate and electrolyte.

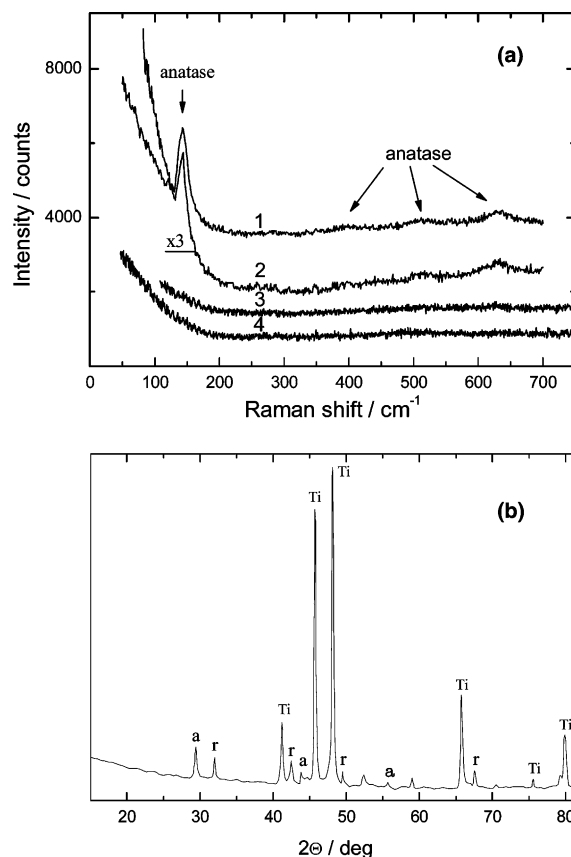


Fig. 9. (a) Raman spectra of the anodic films prepared by the pulsed discharge (2,4) and galvanostatic oxidation (1,3). The film thickness was ca. 50 nm (3,4) and 130 nm (1,2). (b) X-ray diffractogram of the anodic film on titanium prepared by the pulsed discharge method. The film thickness was ca. 300 nm.

The supplied heat involves two components: the heat liberated in the course of chemical reactions and the joule heating effect of the current flow, I ,

$$Q = \sum \Delta H_i + \Delta UI,$$

where $\sum \Delta H_i$ is the sum of the enthalpies of the chemical reactions proceeding at or near the electrode surface, and ΔU the voltage drop across the near-electrode region. The joule heating prevails among the other components, because a huge voltage drop is localized in the areas with low conductivity (gas envelope or growing anodic film). The overall rise in temperature can cause an increase in conductivity of titanium ions in the anodic film, i.e., intensification of its growth [41]. The liberated heat may be sufficient for melting of the film material. Probably, this effect is responsible for the appearance of flowed surface patterns at the electrodes treated repeatedly by the pulsed discharge (Fig. 8(b)).

After reaching the peak value, current falls abruptly (Fig. 2) causing rapid drop of the temperature and condensation of the components of the plasma layer. A very high rate of cooling, which can reach 10^8 K s^{-1} [14], may be responsible for the stabilization of the amorphous state of PD oxide film. Crystalline phases appear only in relatively thick PD anodic films probably as a result of many repetitive heating–cooling cycles.

3.5. Semiconducting properties of anodic films

It is well known that the structure and electronic properties of anodic films on titanium as well as on other valve metals depend strongly on the film growth rate [26,31–38]. Since these properties are very important for possible practical applications of anodic films, many researchers have investigated them using different methods including impedance [26,33,34,36,42–45] and photoelectrochemical techniques [7,26,33,37,38,44–50]. Impedance studies showed that anodic oxide films on titanium are highly doped with donor densities, N_d , ranging from 5×10^{19} to 10^{21} cm^{-3} [26,33,36,42–45,47,50]. However, analysis of impedance data was noted to be complicated by the non-ideal Mott–Schottky behavior of anodic films [33,44,51]. Strongly disordered structure of the anodic films should be taken into account to explain these experimental results [26,42,43]. The donor density of the titanium anodic films was revealed to depend on its growth rate. Ohtsuka and Otsuki [36] found that the dielectric constant increases and the donor concentration decreases with increasing the growth rate of the film. Similar results were also obtained by Blackwood and Peter [33].

Photocurrent spectroscopy is the other useful in situ technique, which was repeatedly applied to examine semiconducting properties of anodic films [7,47]. A marked dependence of the photoelectrochemical properties of titanium anodic films on the film formation

conditions was observed [7,26,33,37,38,45–49]. A comprehensive study of the influence of the formation potential and, hence, the film thickness on photocurrent spectra and photocurrent–potential dependences for galvanostatically prepared films was performed by Leitner et al. [46]. They concluded that thin films formed at lower potentials ($<15 \text{ V}$) was amorphous and demonstrated enhanced indirect band gap values and the absence of a direct band gap. Films of intermediate thicknesses began to demonstrate crystalline properties but had substantially reduced quantum yields of photocurrent, suggesting enhanced surface recombination. Thick films formed at $E > 50 \text{ V}$ were fully crystallized and demonstrated properties similar to those of bulk crystalline TiO_2 . Similar results were also obtained by March and Gorse [49].

In this section, photoelectrochemical and impedance techniques were applied to investigate semiconducting properties of the PD and GS anodic oxide films grown on titanium in sulfuric acid solutions.

3.5.1. Potential dependence of the photocurrent

Fig. 10 shows the comparison of photocurrent (i^{ph}) vs. potential (E) curves recorded at different wavelengths for the thin (25 nm) and thicker (125 nm) anodic films which were prepared by the pulsed discharge and galvanostatic methods. As can be seen from Fig. 10, the shape of $i^{\text{ph}}-E$ curves is markedly dependent on the light wavelength.

For thin PD films the shape is changed from sub- to supra-linear with increasing the illumination wavelength

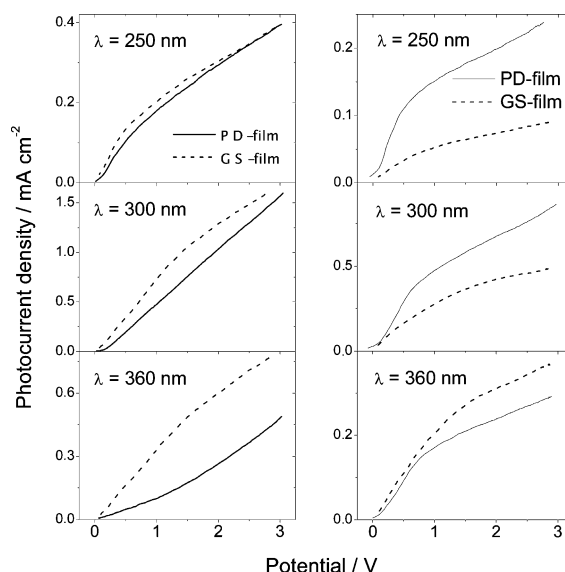


Fig. 10. Potential dependences of the photocurrent recorded at different wavelengths for the 25 nm (left column) and 125 nm (right column) thick anodic TiO_2 films prepared by the high-voltage discharge oxidation (solid lines) and galvanostatically grown (dashed lines). The potential sweep rate was 10 mV s^{-1} . Electrolyte: $1 \text{ M H}_2\text{SO}_4$ solution.

(Fig. 10, left column). For thicker films sub-linear curves are observed irrespective of the wavelength (Fig. 10, right column). We also measured photocurrent vs. potential curves for titanium anodic films grown galvanostatically in the same electrolyte. These dependences for the GS films shown in Fig. 10 demonstrate the general trends similar to those of the PD films with the difference that the supra-linear shape of $i^{\text{ph}}-E$ curves is not observed for thin GS films.

The similar influence of the energy of incident photons on the shape of photocurrent vs. potential curves was reported previously for anodic films on titanium and other valve metals [26,46,52,53] and was associated with the effect of geminate recombination in low mobility materials [52,53]. Because of the low mobility, the photogenerated carriers in such materials do not pass during the thermalization time a distance long enough to prevent their recombination. In this case, the efficiency of free charge generation is less than unity and it contributes to lowering the photocurrent quantum yield together with other losses characteristic of crystalline materials. According to theoretical considerations based on Onsager's theory of geminate recombination, the efficiency of free carrier generation rises with increasing electric field, photon energy of incident light, mobility of photocarriers and temperature [52,54].

The stronger influence of the photon energy on the shape of $i^{\text{ph}}-E$ curves is observed for thin PD films in comparison to the GS films with a comparable thickness. These results could be rationalized by more amorphous or disordered structure of thin PD films. Thick anodic films prepared by both methods demonstrate a similar behavior: the $i^{\text{ph}}-E$ curves at different wavelengths (Fig. 10, left column). Such behavior can be explained in terms of the Butler–Gartner model for crystalline semiconductors [15]. Because of the higher mobility of photogenerated carriers in crystalline materials, no influence of the photon energy is expected on the photocurrent–potential dependences. Thus, the crystallization of the anodic films can be responsible for changing their photoelectrochemical behavior with increasing the thickness. This conclusion is in accordance with our structural studies reported in Section 3.4.

3.5.2. Photocurrent spectra

Fig. 11 presents typical photocurrent spectra measured for the PD and GS films with different thickness. For thin PD films, a marked hypsochromic shift of the long wavelength photocurrent edge is observed. The increase in thickness of the PD film results in a significant shift of the spectrum edge to lower photon energies and in a marked increase of the photocurrent quantum yield (η). Unlike the PD films, the increase in thickness of the GS films from 25–50 to 70–130 nm results in the significant lowering of the photocurrent at $\lambda < 310$ nm and the maximum of the spectrum is shifted to 320 nm. Such

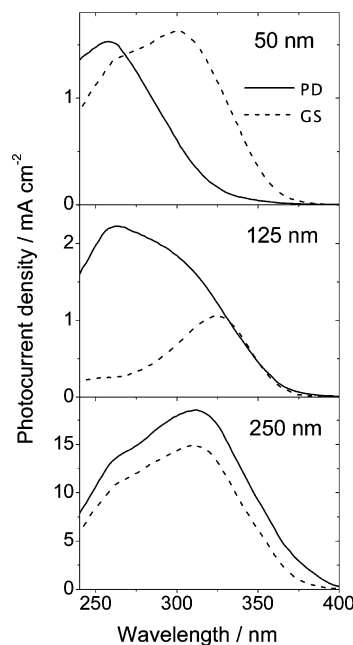


Fig. 11. Photocurrent spectra of the pulsed discharge prepared and galvanostatically grown anodic TiO_2 films with different thickness (50, 125 and 250 nm). The spectra were recorded at a potential of 1.0 V. Electrolyte: 1 M H_2SO_4 solution.

photoelectrochemical behavior of the anodic films on titanium, which has been previously reported, is indicative of enhancing surface recombination, since photons of higher energy are absorbed close to the surface where the effects of surface recombination have a predominant influence on the photocurrent. Peter et al. [24,47] revealed that the film breakdown occurs in this thickness range during the growth of the anodic oxide films on titanium. They attributed the sharp reduction of the photocurrent at shorter wavelengths to the increased rate of recombination and carrier trapping in the stressed and damaged oxide after its breakdown. For thick GS films ($d = 200\text{--}250$ nm), the photocurrent increases considerably, especially at higher photon energies, and the photocurrent spectra again become to be similar to those of the PD films.

For determining bandgap energies, E_g , from the photocurrent spectra, the following relationship between the photocurrent quantum yield, η , and the photon energy, $\hbar\omega$, is commonly used:

$$\eta\hbar\omega = A_n(\hbar\omega - E_g)^{1/n}, \quad (2)$$

where A_n is the constant, $n = 1/2$ and 2 for allowed indirect and direct optical transitions, respectively [15]. This expression is correct when η is directly proportional to the absorption coefficient, α , of the semiconductor. The latter condition is commonly fulfilled for relatively small values of α ($10^2\text{--}10^4 \text{ cm}^{-1}$), i.e., in the vicinity of the absorption edge. Using the Eq. (2), the band gap values can be estimated by extrapolation of the $(\eta\hbar\omega)^{1/n}-\hbar\omega$ curves on the $\hbar\omega$ -axis.

Both PD and GS anodic films exhibit rather extended linear parts of the photocurrent spectra plotted in $(\eta\hbar\omega)^2 - \hbar\omega$ and $(\eta\hbar\omega)^{1/2} - \hbar\omega$ coordinates. Extrapolation of the linear part onto $\hbar\omega$ -axis allows direct estimation of E_{gd} or E_{gi} values. The results of these calculations are listed in Table 1. It should be noted that the linear regions in $(\eta\hbar\omega)^{1/2} - \hbar\omega$ plots do not overlap those in $(\eta\hbar\omega)^2 - \hbar\omega$ plots. The E_{gd} or E_{gi} values obtained for the GS films are in good agreement with those reported by other researchers for the anodic films prepared by similar method [26,46]. The higher band gaps of thinner films can be explained by their amorphous structure as assumed previously [7,26,46]. Although the optical transition selection rules break down for amorphous semiconductors, it has been shown that Eq. (2) is still applicable for these materials and is considered as an empirical relationship [7,55]. In this case the estimated E_{gi} value does not necessarily mean an indirect band gap, as for crystalline semiconductors, and can be regarded as a mobility gap. At the film thickness is more than 80–100 nm, crystallization of the GS anodic films takes place and the E_g decreases to the values (~ 3.2 eV) characteristic of crystalline anatase (Table 1).

For thin anodic films ($d < 100$ nm) obtained by the pulsed discharge method, markedly higher E_{gd} or E_{gi} values are observed as compared with those for the GS films. This difference in E_g practically disappears for thicker films prepared by both methods, which is probably related to the film crystallization. The enhanced apparent band gap values for thin PD films can be caused by a higher structural and chemical disorder in these samples. However, the differential capacitance measurements, as will be shown below, demonstrate that the donor concentration is significantly lower in the PD films compared to the GS films. The other explanation of the higher band gap energies can be in a peculiar structure of the PD grown films including a marked amount of electrolyte anions (~ 5 at.% of sulphur as SO_4^{2-} ions according to Auger analysis) and, probably, structural water. The presence of such inclusions can give rise to an essential change in semiconducting properties of anodic films [36].

Table 1

Direct, E_{gd} , and indirect, E_{gi} , band gaps estimated from photocurrent spectra for anodic TiO_2 films with different thickness prepared by the high-voltage pulsed discharge and galvanostatic anodization in 1 M H_2SO_4 solution

Film thickness (nm)	E_{gd} (eV)		E_{gi} (eV)	
	PD films	GS films	PD films	GS films
25 ± 5	3.93	3.78	3.35	3.27
50 ± 5	4.19	3.66	3.53	3.27
125 ± 10	3.74	–	3.22	3.26
170 ± 10	3.64	3.54	3.19	3.21
250 ± 20	3.52	3.55	3.03	3.15

3.5.3. Differential capacitance measurements

The Mott–Schottky plots obtained from the capacitance (C) vs. potential (E) dependences for the PD and GS anodic films show certain non-linearity in a broad potential region (Fig. 12).

Similar behavior has been previously reported for anodic films on titanium [26,33,36,42,44,51,56–58] and received an ambiguous interpretation. Allard et al. [57] have assigned it to a field dependence of the relative permittivity of the oxide. However, there are several other explanations of such behavior. Thus, the presence of multiple donor levels in the film might result in the non-linear Mott–Schottky plots. In this case, the concentration of ionized donors increases with increasing the electrode potential as the Fermi level shifts down from the conduction band toward the valence band [51]. Moreover, at higher potentials, the passive film can be totally depleted of charge carriers when the space charge region becomes comparable with the film thickness. A more probable explanation of the non-linear C^{-2} – E curves is that the concentration of donors varies through the film thickness. The donor density is the highest at the metal–oxide interface and decreases towards the oxide–electrolyte interface. Such a change in stoichiometry of the anodic films is supported by the results of Auger (Fig. 7) and RBS measurements [58–60].

We found that the differential capacitance (C) of both PD and GS anodic films was somewhat frequency-dependent. However, the frequency dependencies were

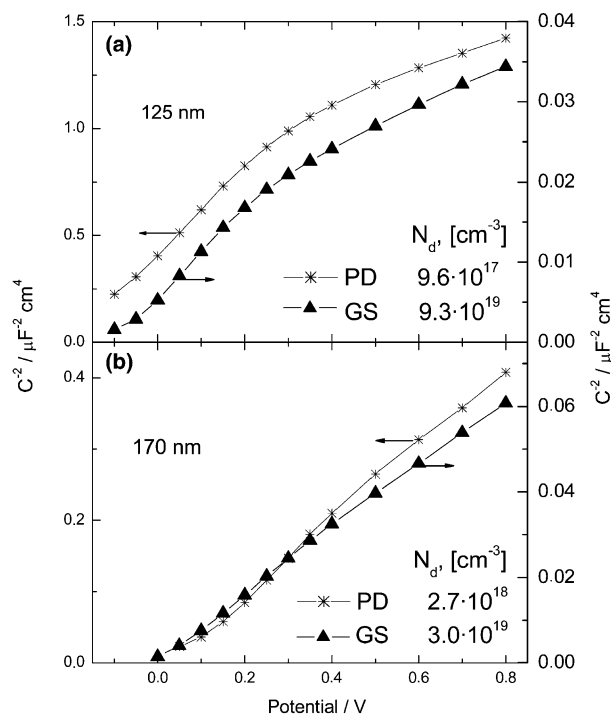


Fig. 12. Mott–Schottky plots of the pulsed discharge prepared and galvanostatically grown anodic TiO_2 films with different thickness (125 and 170 nm). Electrolyte: 1 M H_2SO_4 solution.

similar for PD and GS films. Therefore, all capacitance–potential curves were recorded at 1 kHz, allowing to make a reasonable comparison of the parameters obtained from the impedance data for both types of anodic films.

Assuming $\varepsilon = 56$ [43,61], we calculated the ionized donor concentration from the slope of linear parts of the C^{-2} – E curves observed in more negative potential region. Similar approach has been previously applied in a number of works [33,36,44,56–58]. Donor concentrations of the PD films are significantly lower than that of the GS films and ranges from 10^{17} to 10^{19} cm $^{-3}$, whereas the N_d for the GS films falls in the range from 10^{19} to 10^{20} cm $^{-3}$. Note that the donor concentration depends on the film thickness. The N_d value of the GS films falls from 9.3×10^{19} to 3×10^{19} cm $^{-3}$ whereas in the case of PD films it increases from 9.6×10^{17} to 2.7×10^{18} cm $^{-3}$ at increasing film thickness from 125 to 170 nm.

Such significant differences in the N_d for GS and PD films cannot be interpreted only by a possible difference in the relative dielectric constant for two types of the anodic films. Indeed, thin titanium anodic films grown by traditional methods have been previously shown [26,33,42,44] to be highly defective. Moreover, these films are characterized by a rather extended metal–oxide interface, i.e., a wide region of the non-stoichiometric composition is present in the film [58–60], which is responsible for the high donor density. According to the Auger spectroscopy data (Fig. 7), the anodic films prepared by the pulsed discharge method are practically stoichiometric and have a markedly shorter transition region from TiO $_2$ to Ti, which is consistent with the impedance and photocurrent spectroscopy results. The improved electronic and photoelectrochemical properties of the relatively thin PD anodic films can be caused by extremely high rates of the film growth under conditions of the generation of hot plasma at the electrode–electrolyte interface.

4. Conclusions

The application of a high-voltage pulsed discharge method for preparing thin anodic films on titanium has been proposed in the present work. The capacitor discharge into an electrochemical cell consisting of two titanium electrodes and 1 M aqueous solution of H $_2$ SO $_4$ as an electrolyte was applied for the Ti anodization.

It was revealed that the anodic oxidation of titanium was accompanied by a light flash at the electrode surface and generation of a shock wave. The current and emission transients have a peak, with the time at the peak and the duration being dependent on the parameters of the electrochemical cell, the capacitance value and the applied voltage. Spectroscopic measurements

showed that hot plasma is created near the electrode surface during the Ti oxidation. Overfaradaic yields of the anodic film formation were revealed for the pulsed discharge method and this effect was associated with the participation of high-energy radicals, generated in hot plasma, in the oxide growth process.

The results of Auger depth profiling showed that the anodic films obtained by the pulsed discharge method are characterized by a higher stoichiometry, a more homogeneous composition through the film thickness and a higher content of sulphur probably in the form of SO $_4^{2-}$ ions in comparison to the films prepared by the conventional galvanostatic method. Thin PD films ($d < 50$ nm) have an amorphous structure, whereas the anatase crystalline phase appears in the thicker films ($d = 100$ – 150 nm). However, the decrease in the oxide crystallinity for the films with a comparable thickness was observed in going from the galvanostatically prepared films to ones obtained by the pulsed discharge method. The TiO $_2$ films (50–150 nm) formed in the pulsed regime exhibit significantly higher photocurrent quantum yields at low wavelengths $\lambda < 310$ nm. The films prepared by the pulsed discharge method exhibit a lower donor density compared to galvanostatically grown ones. The maximum difference in the donor concentration of about two orders magnitude is observed for the films with intermediate thickness (100–130 nm).

Acknowledgments

We are grateful to Dr. M.P. Samtsov for assistance with Raman spectroscopy measurements, Dr. L.S. Ivashkevich and Dr. A.S. Lyahov for help with XRD investigations. This work was supported by the Basic Research Foundation of Belarus (Grant No. X02-061).

References

- [1] L. Young, Anodic Oxide Films, Academic Press, London, 1961.
- [2] D.A. Vermilyea, in: P. Delahay (Ed.), Advanced Electrochemistry and Electrochemical Engineering, vol. 3, Interscience, New York, 1963.
- [3] J.W. Diggle (Ed.), Oxides and Oxide Films, vol. 1, Dekker, New York, 1972.
- [4] E.J. Kelly, in: J.O'M. Bockris, E. Yeager, R.E. White (Eds.), Modern Aspects of Electrochemistry, vol. 4, Plenum Press, New York, 1984.
- [5] S.R. Morrison, Electrochemistry of Semiconductors and Oxidized Metal Electrodes, Plenum Press, New York, 1980.
- [6] A. Aladjem, J. Mater. Sci. 8 (1973) 688.
- [7] U. Stimming, Electrochim. Acta 31 (1986) 415.
- [8] G.C. Wood, C. Pearson, Corros. Sci. 7 (1967) 119.
- [9] J. Yahalom, J. Zahavi, Electrochim. Acta 15 (1970) 877.
- [10] C.K. Dyer, J.S.L. Leach, J. Electrochem. Soc. 125 (1978) 1032.
- [11] V. Kadary, N. Klein, J. Electrochem. Soc. 127 (1980) 139.
- [12] V.V. Bakovets, O.V. Polyakov, I.P. Dolgovesova, Plasma Electrolytic Anodic Treatment of Metals, Nauka, Novosibirsk, 1991.

- [13] V.I. Chernenko, L.A. Snezhko, I.I. Papanova, Coating Preparation by Anodic Spark Electrolysis, Khimiya, Leningrad, 1991.
- [14] A.L. Yerokhin, X. Nie, A. Leyland, A. Matthews, S.J. Dowey, Surf. Coat. Tech. 122 (1999) 73.
- [15] Yu.V. Pleskov, Yu.Ya. Gurevich, Semiconductor Photoelectrochemistry, Consultants Bureau, New York, 1986.
- [16] F.M. Phelps, MIT Wavelength Tables, vol. 2, The M.I.T. Press, Cambridge, MA, 1982.
- [17] S.B. Radovanov, I.D. Holclajtner-Antunovich, M.R. Tripkovic, Plasma Chem. Plasma Process. 6 (1986) 457.
- [18] S.B. Radovanov, M.R. Tripkovic, I.D. Holclajtner-Antunovich, Contrib. Plasm. Phys. 26 (1986) 389.
- [19] K. Kobayashi, Y. Tomita, M. Sanmyo, J. Phys. Chem. B 104 (2000) 6318.
- [20] L.Z. Boguslavsky, S.A. Khainatsky, A.N. Shcherbak, Tech. Phys. 46 (2001) 43.
- [21] H.J. Mathieu, J.B. Mathieu, D. Lanbolt, J. Vac. Sci. Technol. 14 (1977) 1023.
- [22] D. Laser, M. Yaniv, S. Gottesfeld, J. Electrochem. Soc. 125 (1978) 358.
- [23] D.J. Blackwood, R. Greef, L.M. Peter, Electrochim. Acta 34 (1989) 875.
- [24] J.F. McAleer, L.M. Peter, J. Electrochem. Soc. 129 (1982) 1252.
- [25] G. Blondeau, M. Froelicher, M. Froment, A. Hugot-Le Goff, Thin Solid Films 42 (1977) 147.
- [26] S. Piazza, L. Cala, C. Sunseri, F. Di Quarto, Ber. Bunsen. Phys. Chem. 101 (1997) 932.
- [27] A. Hickling, in: J.O'M. Bockris, B.E. Conway (Eds.), Modern Aspects of Electrochemistry, vol. 6, Butterworths, London, 1971.
- [28] K. Harada, S. Suzuki, Nature 266 (1977) 275.
- [29] S.K. Sengupta, R. Singh, A.K. Srivastava, J. Electrochem. Soc. 145 (1998) 2209.
- [30] G. Jouve, A. Politi, P. Lacombe, G. Vuye, J. Less-Common. Met. 59 (1978) 175.
- [31] J.S.L. Leach, B.R. Pearson, Electrochim. Acta 29 (1984) 1263.
- [32] J.-L. Delplancke, R. Winand, Electrochim. Acta 33 (1988) 1539.
- [33] D.J. Blackwood, L.M. Peter, Electrochim. Acta 34 (1989) 1505.
- [34] T. Shibata, Y.-C. Zhu, Corr. Sci. 37 (1995) 253.
- [35] T. Ohtsuka, N. Nomura, Corr. Sci. 39 (1997) 1253.
- [36] T. Ohtsuka, T. Otsuki, Corr. Sci. 40 (1998) 951.
- [37] M. Mikula, J. Blecha, M. Ceppan, J. Electrochem. Soc. 139 (1992) 3470.
- [38] M.R. Kozlowski, P.S. Tyler, W.H. Smyrl, R.T. Atanasoski, Surf. Sci. 194 (1988) 505.
- [39] I.R. Beattie, T.R. Gilson, Proc. Roy. Soc. Lond. Ser. A 307 (1968) 407.
- [40] A. Felske, W.J. Plieth, Electrochim. Acta 34 (1989) 75.
- [41] J.-C. Marchenoïn, J.-P.L. Masson, CR. Acad. Sci. 289 (1986) 145.
- [42] C. Fonseca, S. Boudin, M.C. Belo, J. Electroanal. Chem. 379 (1994) 173.
- [43] C. Fonseca, M.G. Ferreira, M.C. Belo, Electrochim. Acta 39 (1994) 2197.
- [44] J.W. Schultze, U. Stimming, J. Weise, Ber. Bunsen. Phys. Chem. 86 (1982) 276.
- [45] W.A. Badawy, A. Felske, W.J. Plieth, Electrochim. Acta 34 (1989) 1711.
- [46] K. Leitner, J.W. Schultze, U. Stimming, J. Electrochem. Soc. 133 (1986) 1561.
- [47] J.F. McAleer, L.M. Peter, Faraday Discuss. 70 (1980) 67.
- [48] J.W. Halley, M. Kozlowski, M. Michalewicz, W. Smyrl, N. Tit, Surf. Sci. 256 (1991) 397.
- [49] J. Marsh, D. Gorse, Electrochim. Acta 43 (1998) 659.
- [50] A. Goossens, Surf. Sci. 371 (1997) 390.
- [51] E.-J. Lee, S.-I. Pyun, J. Appl. Electrochem. 22 (1992) 156.
- [52] F. Di Quarto, S. Piazza, C. Sunseri, Electrochim. Acta 38 (1993) 29.
- [53] F. Di Quarto, S. Piazza, R. D'Agostini, C. Sunseri, J. Electroanal. Chem. 228 (1987) 119.
- [54] D.M. Pai, R.C. Enck, Phys. Rev. B 11 (1975) 5163.
- [55] N.F. Mott, E.A. Davis, Electronic Processes in Noncrystalline Solids, Clarendon Press, Oxford, 1979.
- [56] G. Nogami, Y. Ogawa, Y. Nishiyama, J. Electrochem. Soc. 135 (1988) 3008.
- [57] K.D. Allard, M. Ahrens, K.E. Heusler, Werkstoff. Korros. 26 (1975) 694.
- [58] D. Zane, F. Decker, G. Razzini, Electrochim. Acta 38 (1993) 37.
- [59] N.R. Armstrong, R.N. Quinn, Surf. Sci. 67 (1977) 451.
- [60] Y. Serruys, T. Sakout, D. Gorse, Surf. Sci. 282 (1993) 279.
- [61] T. Hurlen, S. Hornkjøl, Electrochim. Acta 36 (1991) 189.